JOURNAL OF Applied Polymer SCIENCE

Structural Changes in the Carbon Black Network in Carbon-Black-Filled Styrene-Butadiene Rubber Samples Cured with a Two-Step Process

Atsushi Kato,[1] Yoshinobu Isono[2]

[1]Strategic Service Promotion Department, NISSAN ARC, Limited, 1 Natsushima-Cho, Yokosuka 237-0061, Japan

[2]Department of Materials Science and Technology, Nagaoka University of Technology, Kami-Tomioka 1603-1, Nagaoka, Niigata 940-2188, Japan

Correspondence to: A. Kato (E-mail: kato@nissan-arc.co.jp)

ABSTRACT: The volume resistivity of carbon black (CB)-filled crosslinked styrene-butadiene rubber (SBR) samples cured in two steps and having a fixed elongation condition declined slightly when the elongation ratio (α) was 3 or smaller, whereas the value increased markedly at $\alpha = 4$. Three-dimensional transmission electron microscopy observations revealed that the closest interparticle distance between the carbon black aggregates (CB_{ag}'s) and the CB_{ag} number density decreased at $\alpha = 1-2$ but increased at $\alpha = 4$ and that the distance between the centers of gravity of the closest CB_{ag} and the volume of CB_{ag} increased at $\alpha = 1-3$ but decreased at $\alpha = 4$. Also, the fraction of crosslinked chains of the carbon black network (CB_{net}) was decreased with elongation, and the fraction of branched chains increased. The fraction of isolated chains in particular showed a more pronounced increase at $\alpha > 3$ compared with $\alpha < 3$. These results presumably imply that for the sample with $\alpha > 3$, the coarsened CB_{ag}'s were finely divided and also that the CB_{net} was broken by elongation. © 2012 Wiley Periodicals, Inc. J. Appl. Polym. Sci. 000: 000–000, 2012

KEYWORDS: composites; elastomers; microscopy; morphology; rubber

Received 5 April 2012; accepted 17 July 2012; published online
DOI: 10.1002/app.38356

INTRODUCTION

Polymer nanocomposites are unique materials in that their material properties change substantially with the addition of a small volume fraction of nanometer-sized filler particles.[1–6] The changes are observed when the filler size is comparable to that of the polymer chains and to the average wall-to-wall distance between fillers. Under such conditions and with good filler dispersion in the matrix, it is believed that a secondary network of polymer chains connecting the filler particles forms.[2–5] This transient network is assumed to be the cause of the large enhancement observed in the viscoelastic properties. The transient network also produces rubberlike behavior in a certain range of frequencies.[3] The appearance and range of this regime depend on the polymer–filler affinity and, hence, on the lifetime of attachments between the fillers and bridging chains.

It has been reported in recent years that an electrical network forms among carbon black aggregates (CB_{ag}'s) in sulfur-cured natural rubber (NR) vulcanizates when the carbon black (CB) filler content is 30 phr (grams of additive per 100 g of rubber) or higher.[7–12] This finding is based on the measurement of the closest interparticle distance (d_p) of the CB_{ag}'s with three-dimensional (3D) transmission electron microscopy (TEM) observations, image analysis, and volume resistivity (ρ_v) measurements. These techniques have revealed many new insights, including that the structures of the carbon black network (CB_{net}) consist mainly of crosslinked chains and branched chains and that a certain relationship exists between the fractions of these chains and the CB filler content. Furthermore, two dielectric relaxation components (a circular arc shaped pattern and the remaining relaxation) were isolated from Cole–Cole plots of dielectric relaxation, and a good linear relationship was found to exist between the chain fractions and the fractions of the intensities of these relaxation components.[9] Omnés et al.[13] also suggested that the elastic modulus of CB-filled sulfur-cured NR vulcanizates can be predicted with a morphological model that takes into account bound rubber, occluded rubber, and also the structures of the filler network.

Meanwhile, on the basis of q_v measurements and 3D TEM observations, Kato et al.[14] reported that the CB_{net} in CB-filled crosslinked NR was destroyed when the heat treatment conditions were set to minimize the occurrence of thermal oxidative degradation. It was found that the crosslinked chains of the CB_{net} were broken by the heat treatment process and that the number of branched chains increased. These findings showed

Table I. Recipes for the Preparation of the CB-Filled Cured SBR Reference Samples and the Sample Cured in Two Steps

	Ingredients					
Sample	CB10/SBR[a]	CB20/SBR[a]	CB40/SBR[a]	CB60/SBR[a]	CB80/SBR[a]	CB40/SBR (α)[b]
SBR1502	100	100	100	100	100	100
DCP (phr[c])	3	3	3	3	3	3
CB (phr)[d]	10	20	40	60	80	40
Φ_{CB}[e]	0.050	0.095	0.17	0.24	0.30	0.17

[a]Curing conditions: 30 min at 170°C under pressure of 2 MPa.
[b]Two-step curing conditions: (1) precuring for 8.5 min at 130°C under a pressure of 2 MPa before elongation and (2) postcuring for 15 min at 170°C after elongation.
[c]Grams per 100 g of rubber.
[d]High abrasion furnace (N330).
[e]Calculated with densities of CB and SBR of 1.8 and 0.94.

that 3D TEM observations and image analysis are effective techniques for examining the structural changes that occur in the CB_{net}. Satoh et al.[15] measured the differential dynamic modulus (DDM) and ρ_v values of CB-filled uncured SBRs (i.e., CB-filled SBR compounds) in a wide range of shear strains from 0.001 to 0.5. They found that there was a one-to-one correspondence between the changes in DDM and ρ_v above the percolation threshold; that is, there was no ρ_v change in the linear viscoelasticity, but there was a ρ_v enhancement in the nonlinear viscoelasticity. These results mean that the contact CB filler network exists and the nonlinear viscoelasticity of high-CB-filled rubber is caused by a rupture in the CB filler network. In addition, on the basis of the measurements of DDM in large compression and recovery, they found that the filler network ruptured because of large compression and recovery in shape was attained at a timescale that was closely related to the particle size.[16]

Many of the experimental findings mentioned previously suggested change and recovery in the CB–filler network in large deformation. Now, we have very powerful tools in 3D TEM and the image analysis technique, which give us direct observation of the CB–filler network structure. Therefore, in this study, the change in ρ_v and the structural change in the stretched CB_{net} in CB-filled cured styrene-butadiene rubber (SBR) specimens prepared by a two-step curing method were investigated on the basis of ρ_v measurements, 3D TEM observations, and image analysis.

EXPERIMENTAL

Materials: CB-Filled SBR Cured in Two Steps

Two types of CB-filled cured SBR 1502 were prepared: reference samples and samples cured in two steps. The compounding recipes of the reference samples investigated in this study are given in Table I. The only ingredient that changed in the series of cured SBR samples was the CB loading, which was varied in the range 10–80 phr. The carbon black volume fraction (Φ_{CB}) was calculated with densities of CB[17] and SBR[18] of 1.8 and 0.94 g/cm^3, respectively. The quantity of the compounding agent was the same in all of the cured samples: 3 phr of dicumyl peroxide (DCP). Curing was performed under a pressure of 2 MPa at 170°C for 30 min in a mold.

Table I shows the recipes of the CB-filled SBR 1502 samples cured in two steps, and Figure 1 shows the curing process. The DCP and CB loadings were 3 and 40 phr, respectively. Precuring was performed under a pressure of 2 MPa at 130°C for 8.5 min in a mold. Rectangular specimens (50 mm wide, 70 mm long, and 2 mm thick) were cut from precured SBR sheets. After stretching, the specimens between two marker lines at an arbitrary elongation ratio (α), and the stretched specimens were postcured at 170°C for 15 min. After postcuring, the specimens were released from the chucks and held at room temperature for about 1 h before we measured the distance between the two marker lines. α is defined here as the ratio of the length of the specimen before extension to the length of the specimen after extension. Table II shows the residual elongation ratios (α_{res}) of the CB-filled CB40/SBR samples after two steps of curing (where α is the initial elongation ratio from 1 to 4 after precuring and before postcuring). The α_{res} values of the specimens were 90% or more of the initial α values. Taking into consideration the findings of Kohjiya et al.,[7,8,11,12] Kato et al.,[9,14] Ikeda et al.,[10] and Satoh et al.,[15] we believe that a CB_{net} also formed in the CB40/SBR samples in this study, despite the different kinds of CB and rubber used and the differences in the vulcanizing or curing systems.

Apparatus and Procedure

Measurement of ρ_v. The ρ_v values of the samples were measured with the three-electrode method with an R8340A ultra-high-resistance meter (Advantest Corp., Tokyo, Japan). The three electrodes were made of stainless steel and consisted of a main electrode 50 mm in diameter, a guard electrode with internal/external diameters of 70/80 mm and a counter electrode 103 mm in diameter (TR-43C, Advantest Corp.) An SBR sample cured in two steps was tightly sandwiched between the main

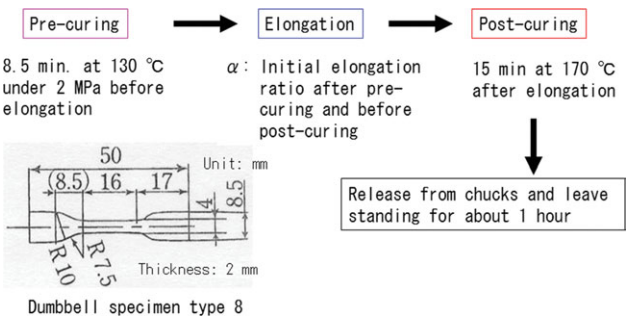

Figure 1. Two-step curing process of the CB-filled cured SBR samples. [Color figure can be viewed in the online issue, which is available at wileyonlinelibrary.com.]

Table II. α_{res} Values of the CB-Filled Cured SBR Samples (α = 1–4) after Two Steps of Curing

Sample	CB40/SBR ($\alpha = 1$)	CB40/SBR ($\alpha = 2$)	CB40/SBR ($\alpha = 3$)	CB40/SBR ($\alpha = 4$)
α	1	2	3	4
α_{res}	1	1.82	2.82	3.77

and guard electrodes and the counter electrode. The guard electrode was grounded to prevent current from flowing along the sample surface. ρ_v was calculated from the current that flowed through the sample when a certain specified voltage was applied. This measurement method conformed to the procedure specified in the relevant Japanese Industrial Standard (JIS K 6911), which is equivalent to ASTM D 257-90. The sample cells were also loaded in a constant-temperature bath, which was used to keep the temperature at a specified level for approximately 20 min. The range of temperature measurement was from 296 to 363 K (23–90°C), and the applied voltage was 100 or 1 V/min. Subsequently, the current that flowed through the sample upon the application of voltage was measured to determine the temperature dependence of ρ_v.

3D TEM Observations. The instrument used in the 3D TEM observations was a Tecnai G2 F20 TEM (FEI Co., Hillsboro, Oregon, USA). The accelerating voltage of the electron beam was set at 200 kV. The samples were tilted over a range of angles from −70 to +70°, and image data (tilted images) were continuously obtained in 2° increments. In total, 71 consecutive tilted images were automatically loaded into the computer. The positions of the tilted images were aligned at that time, and a search was made for their axis of rotation. These tilted images were not simply two-dimensional image slices but rather two-dimensional projected images of the mass–density distribution of the samples. Using IMOD software (a program created at Colorado University)[19] installed on the TEM, we converted the consecutive tilted images thus obtained into image slices showing the mass–density distribution at each angle. Then, 3D images were reconstructed from the image slices by application of a radon transform with the Amira software developed by TGS, Inc, Irvine, California, USA.[20]

Simultaneously, volume rendering or surface rendering was performed to construct the 3D images on a nanometer scale.[21] The former method reconstructs a 3D object by stacking cross-sectional images vertically and displaying the data semitransparently. The latter method reconstructs a 3D object by extracting the contours of the object depicted in a cross-sectional image in terms of curves and inserting surfaces between many of the curves thus obtained.

The principle of 3D TEM is virtually the same as that of X-ray computed tomography. Because an electron beam is used, this technique is also called *electron beam tomography*. The use of 3D TEM not only facilitates the 3D visualization of nanoparticles, it also makes it possible to calculate their number, density, 3D shape, volume, and other details.[7–12,22–28] Because it is well known that organic polymers are apt to be damaged by electron beams,[29] this is an issue that must always be kept in mind when one makes 3D TEM measurements.

RESULTS AND DISCUSSION

Relationship between the ρ_v and Temperature of the SBR Cured in Two Steps

Figure 2(a) shows the ρ_v's measured in a temperature range of 22–90°C for the CB-filled crosslinked SBR samples having fixed αs of 1–4, respectively. At 22°C, the samples with αs of 1–3 showed a slight decline in ρ_v with increasing α, whereas ρ_v increased markedly at $\alpha = 4$. This slight decline in ρ_v at α = 1–3 and the pronounced increase at $\alpha = 4$ presumably occurred because of the changes in the distribution of the CB_{ag}'s. These characteristics are described in more detail later, in the discussion of the 3D TEM observations. Moreover, all of the samples showed a decline in ρ_v with increasing temperature; this was

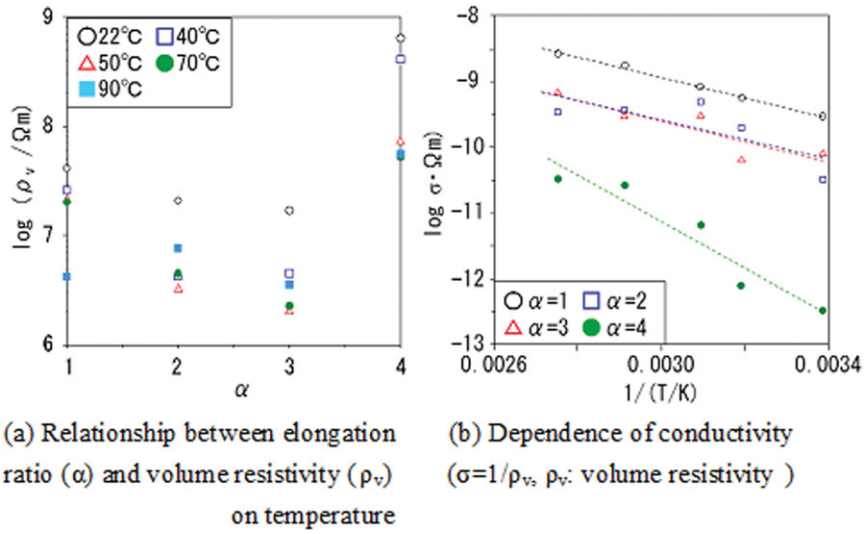

(a) Relationship between elongation ratio (α) and volume resistivity (ρ_v) on temperature

(b) Dependence of conductivity ($\sigma=1/\rho_v$, ρ_v: volume resistivity)

Figure 2. σ values of the CB-filled SBR samples cured in two steps. [Color figure can be viewed in the online issue, which is available at wileyonlinelibrary.com.]

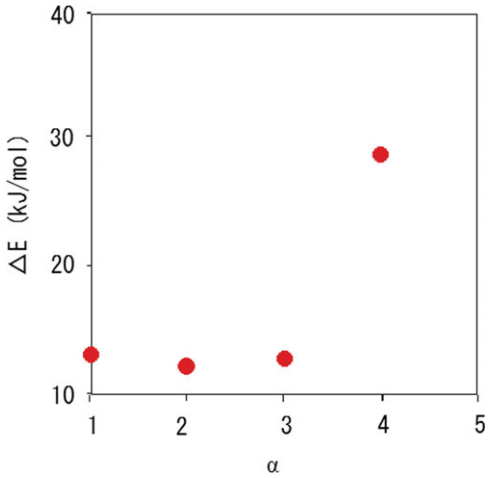

Figure 3. Relationship between ΔE of σ and α. [Color figure can be viewed in the online issue, which is available at wileyonlinelibrary.com.]

attributed to the process of thermal activation. Figure 2(b) presents Arrhenius plots, which show the logarithm of the electrical conductivity ($\sigma = 1/\rho_v$) plotted against the inverse of the absolute temperature (T). For all of the samples with αs of 1–4, a nearly linear relationship was seen between log σ and $1/T$. The activation energy (ΔE) of this conductivity could be found from the gradient of the straight-line approximations in the figure. Figure 3 shows ΔE as a function of α. For the samples with αs of 1–3, ΔE was low and was nearly the same in all three cases, but for the sample with an α of 4, ΔE was markedly higher. These results suggest that at $\alpha = 4$, that is, for an α larger than 3, the electrical network of the CB_{ag}'s in the rubber was destroyed.

Distribution of the CB_{ag}'s in the Reference Specimens and the Specimens Cured in Two Steps

Figure 4 shows 3D TEM images of the CB10, CB20, CB40, and 80/SBR reference samples. The white grains are CB_{ag}'s. In the CB10/SBR sample, CB_{ag}'s were observed here and there in the image. At CB loadings higher than 10 phr, the CB_{ag} structures continued to grow larger in size and tended to be nearly

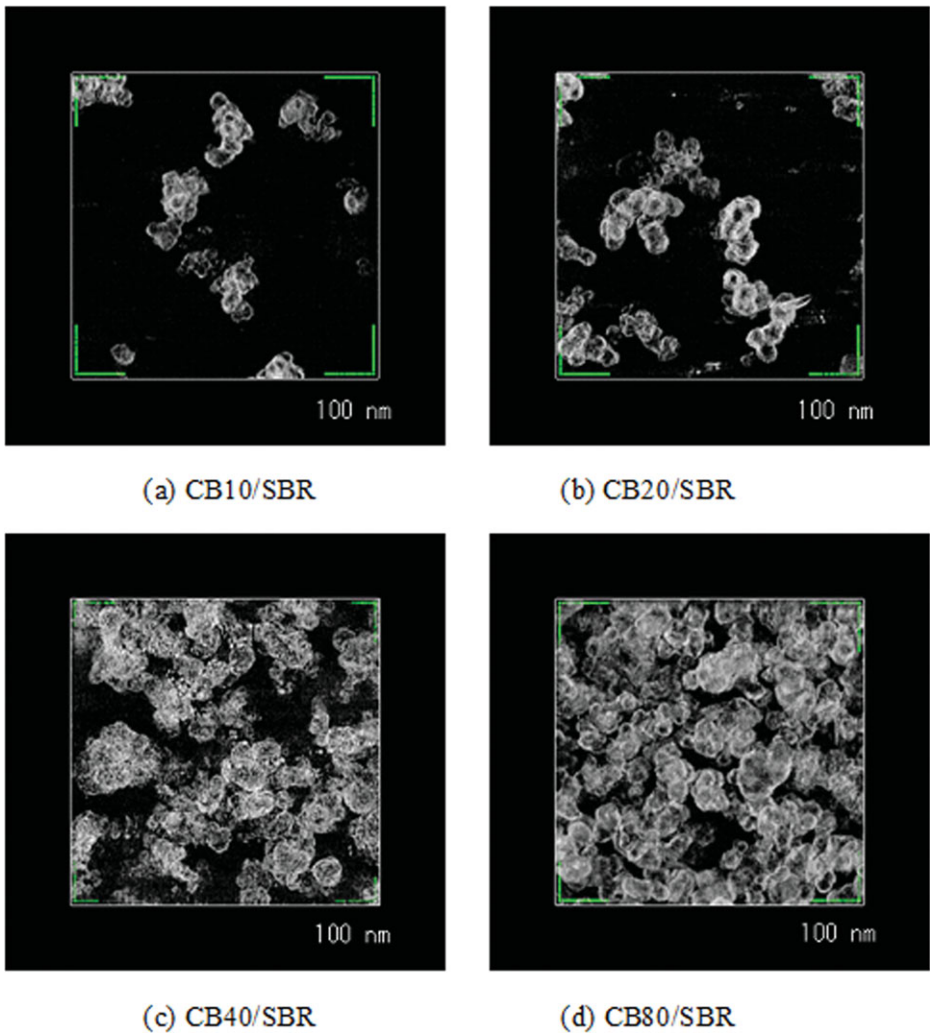

Figure 4. 3D TEM images of the CB-filled cured SBR reference samples. [Color figure can be viewed in the online issue, which is available at wileyonlinelibrary.com.]

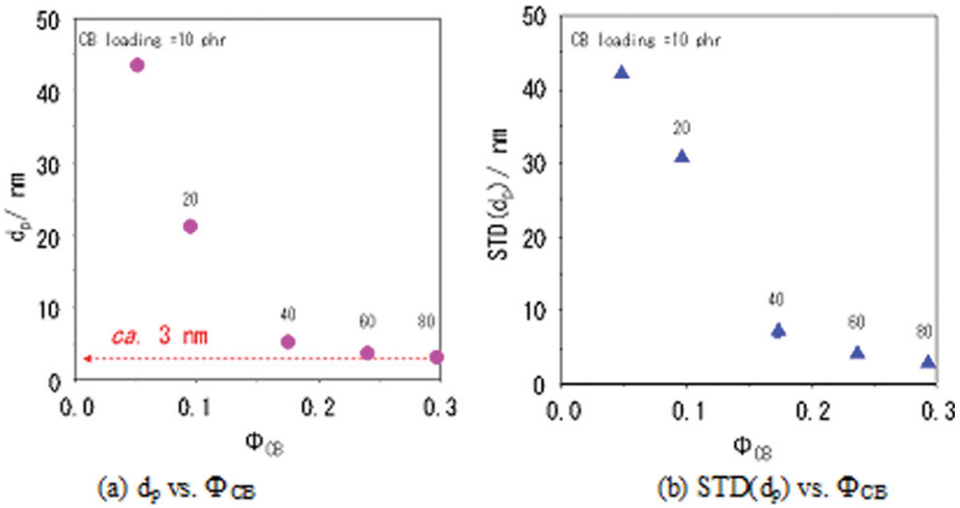

Figure 5. Dependence of the average closest d_p between the CB_{ag}'s and STD (d_p) on Φ_{CB}. [Color figure can be viewed in the online issue, which is available at wileyonlinelibrary.com.]

uniformly distributed in the CB80/SBR samples. By applying a 3D image analysis technique to the images in Figure 4, we determined the closest d_p between CB_{ag}'s and its standard deviation [STD (d_p)], as proposed by Kato and coworkers.[7–12,14,24,26,27]

Figure 5(a, b) shows the dependence of d_p and STD (d_p) on $\Phi_{CB,}$ respectively. It is seen in Figure 5(a, b) that d_p and STD (d_p) decreased as Φ_{CB} increased above 0.050 (10 phr) and that both values stabilized at Φ_{CB}'s of 0.17 (40 phr) or higher. The stable value of d_p was approximately 3 nm, which was identical to the value reported for high abrasion furnace-filled sulfur-cured NR vulcanizates.[7–12,14,24,26,27] These results imply the presence of a CB/SBR interaction layer that prevented direct contact between the CB_{ag}'s even when Φ_{CB} was increased. We assumed that this interaction layer was closely related to the bound rubber phase. As described later, the linking of the CB_{ag}'s at a distance of 3 nm resulted in the formation of a CB_{net} consisting of crosslinked, branched, and isolated chains. In Figure 5(b), which shows the dependence of STD (d_p) on $\Phi_{CB,}$ we observed that the CB_{ag}'s became more uniformly distributed at Φ_{CB} values above 0.050 and that the samples were filled with CB at approximately the distance of the CB/SBR interaction layer at Φ_{CB} of 0.17 or higher.

Figure 6 shows the 3D TEM images of the CB40/SBR samples cured in two steps and having α values in the range 1–4. The elongation direction is along the horizontal axis, and the white grains are CB_{ag}'s. We observed that the gaps between the CB_{ag}'s tended to increase with increasing α. In particular, at $\alpha = 4$, the CB_{ag}'s exhibited a segmented morphology. These results presumably support the pronounced increase seen in ρ_v for $\alpha = 4$. Figure 7 shows d_p and the distance between the centers of gravity of the closest carbon black aggregates (d_g's) as a function of α.[7–12,14,24,26,27] Surprisingly, the d_p values of the samples with αs of 1–2 decreased slightly, whereas it increased for the samples with a larger α value. These results imply that for the samples with αs of 1–2, their cross-sectional area decreased with elongation and, thereby, pushed the CB_{ag}'s toward the interior of the sample. This resulted in a highly packed state that reduced d_p slightly; ρ_v also declined somewhat. At α values greater than 2, the elongation probably pulled the CB_{ag}'s apart. This resulted in a pronounced increase in d_p; ρ_v also increased markedly.

Furthermore, we observed that d_g increased at $\alpha = 1$–3 and decreased at $\alpha = 4$. Here, we consider that d_g reflected d_p and the size of the two closest CB_{ag}'s. For the samples with $\alpha = 1$–3, the reduction of the sample cross-sectional area accompanying elongation promoted the coalescence of the CB_{ag}'s, whereas with an α value greater than 3, the shear fields produced by the further reduction of the sample cross-sectional area presumably worked to finely divide the coarsened CB_{ag}'s. The dependence of the aggregate number density (D_{CB}) and the average aggregate volume (V_{CB}) on α is shown in Figure 8. We observed that D_{CB} decreased with α values of 1–3 and increased at $\alpha = 4$. The former result corresponded to the coalescence of the CB_{ag}'s, and the latter result corresponded to the division of the coarser CB_{ag}'s. In addition, V_{CB} increased at α values of 1–3 and decreased at $\alpha = 4$. These results also corresponded well to the CB_{ag} coalescence and the division of coarser CB_{ag}'s.

CB_{net} in the Reference Specimens and the Specimens Cured in Two Steps

The results in Figure 5 show that d_p displayed a constant value of approximately 3 nm when the CB loading was increased to 40 phr or higher. Because this value implied the thickness of the CB/SBR interaction layer, we assumed that the linking of the nearest neighbor CB_{ag}'s at a distance of approximately 3 nm formed the CB_{net}. Accordingly, the CB_{net} could be visualized by the drawing of lines connecting the centers of gravity of these nearest CB_{ag}'s.[7–12,14,24,26,27] Figure 9 presents images of the CB_{net} thus obtained for the CB40/SBR samples cured in two steps with α values of 1–4, respectively. The elongation direction was along the horizontal axis, and bars representing 100 nm are shown in the four corners of each rectangular parallelepiped view. CB_{net}'s that are not connected are shown in different colors. The CB_{net} in the unelongated state ($\alpha = 1$), shown in Figure 9(a), was almost entirely the same color; this indicated that nearly all of the CB_{ag}'s were linked at a distance of approximately 3 nm. In

Applied Polymer SCIENCE

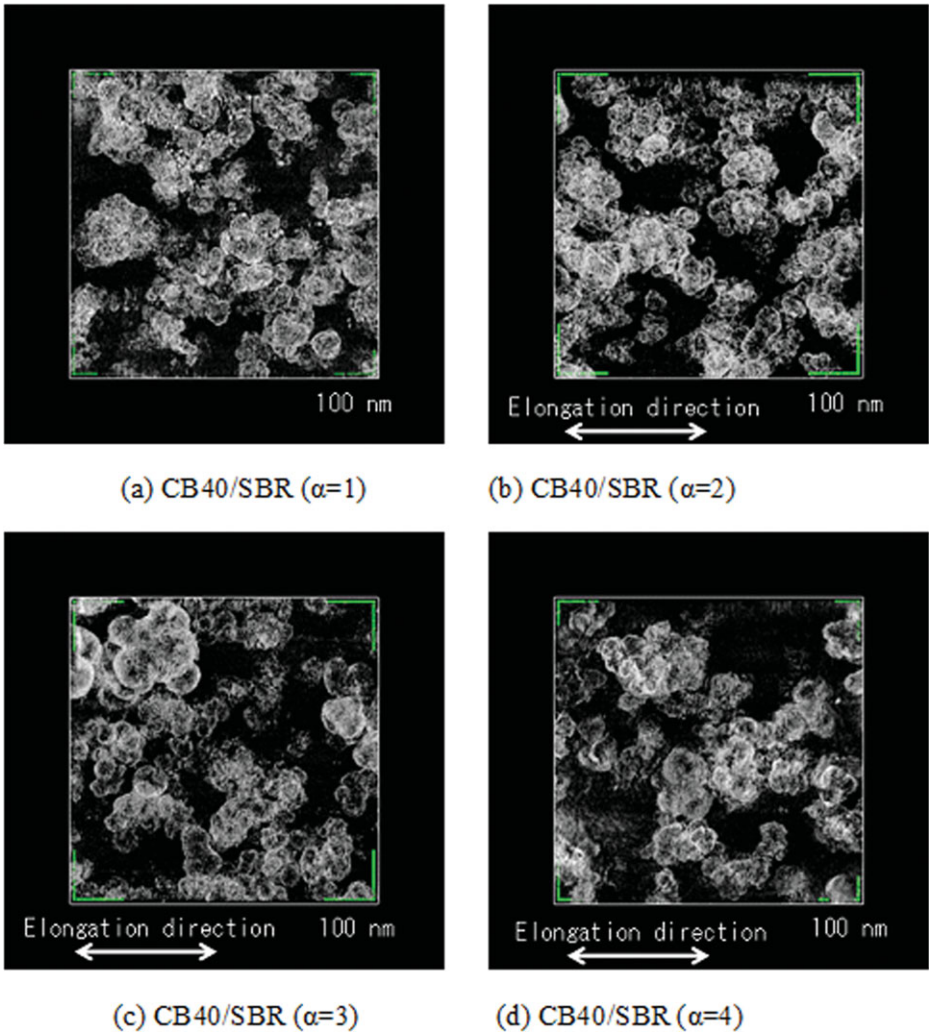

Figure 6. 3D TEM images of the CB-filled SBR samples cured in two steps. [Color figure can be viewed in the online issue, which is available at wileyonlinelibrary.com.]

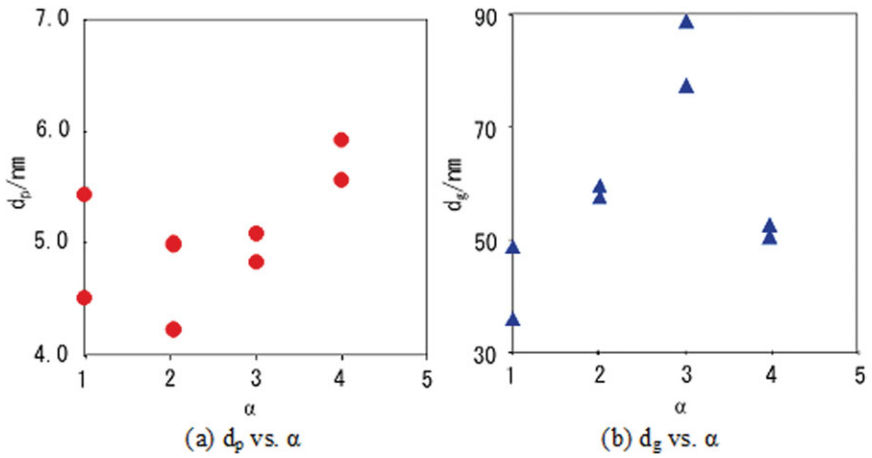

Figure 7. Average closest d_p between CB_{ag}'s and d_g as a function of α. [Color figure can be viewed in the online issue, which is available at wileyonlinelibrary.com.]

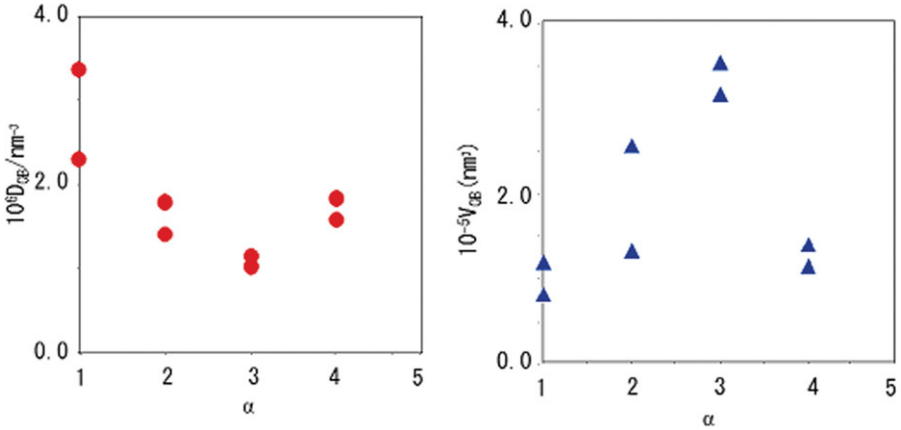

(a) Dependence of CB aggregate number density (D_{CB}) on α

(b) Dependence of CB aggregate average volume (V_{CB}) on α

Figure 8. Dependence of D_{CB} and V_{CB} on α. [Color figure can be viewed in the online issue, which is available at wileyonlinelibrary.com.]

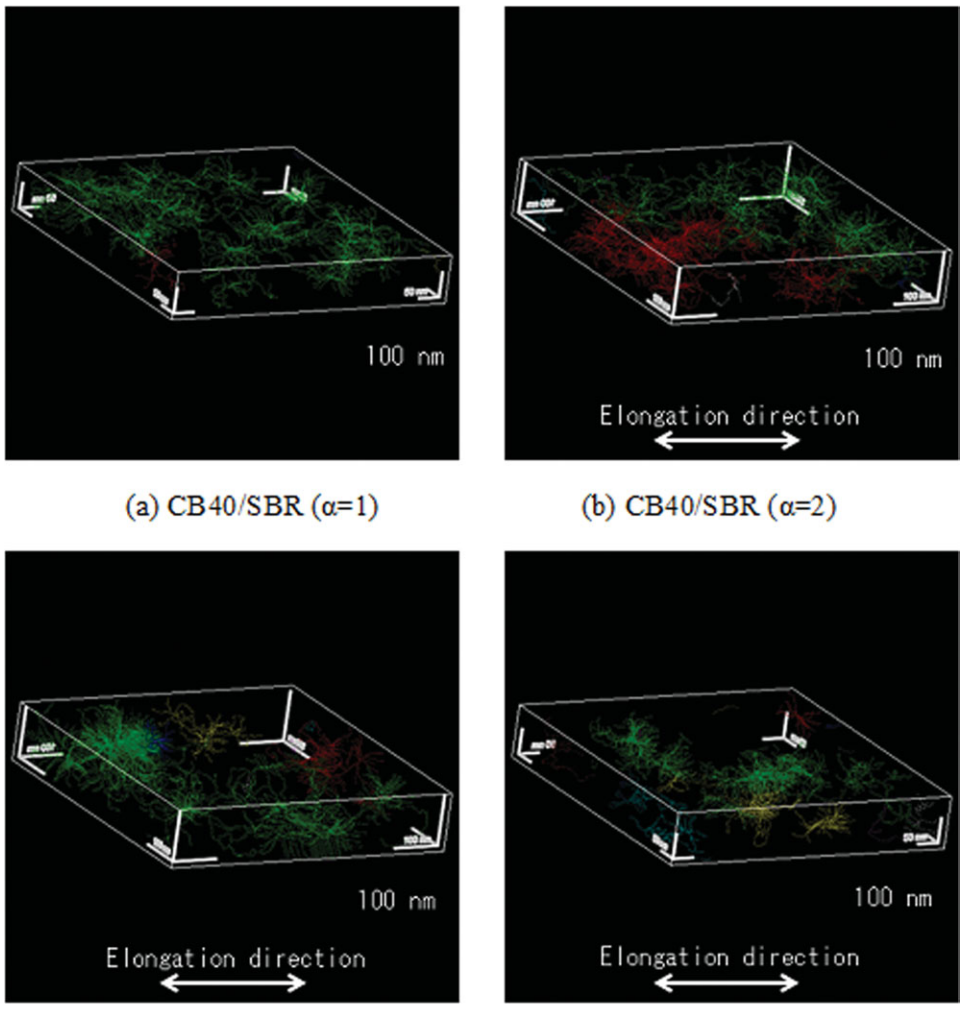

(a) CB40/SBR (α=1)

(b) CB40/SBR (α=2)

(c) CB40/SBR (α=3)

(d) CB40/SBR (α=4)

Figure 9. CB_{net} images of the CB-filled SBR samples cured in two steps. [Color figure can be viewed in the online issue, which is available at wileyonlinelibrary.com.]

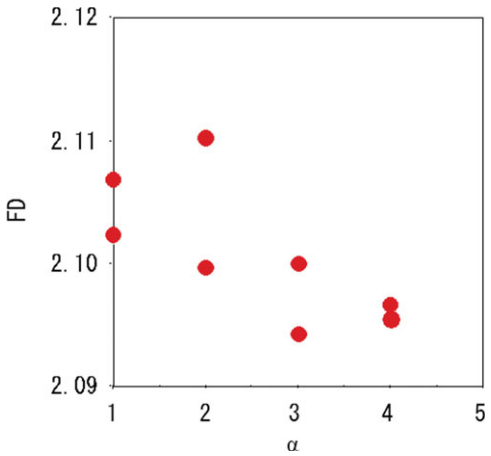

Figure 10. Relationship between the FD of CB_{net} and α. [Color figure can be viewed in the online issue, which is available at wileyonlinelibrary.com.]

contrast, as the samples were increasingly elongated, the CB_{net} colors changed; this implied that the CB_{net} was broken by elongation. The CB40/SBR sample with $\alpha = 4$ in Figure 9(d) in particular was broken up into small fragments.

In addition, the fractal dimension (FD) of the CB_{net} in Figure 9 was calculated by the box counting method.[30–33] FD of the CB_{net} is shown in Figure 10 as a function of α. The results indicate that FD tended to decrease with increasing α. This result suggests that the CB_{net} was flattened as a result of elongation.

The 3D network structure formed by the clustering of the CB_{ag}'s is schematically shown in Figure 11, together with the parameters of the network structures.[7–12,14,24,26,27] The circles in the figure represent the CB_{ag}'s. The thin arrows indicate that the CB chains composed of a few or several aggregates were linked to the surrounding network structures. The two thick arrows show

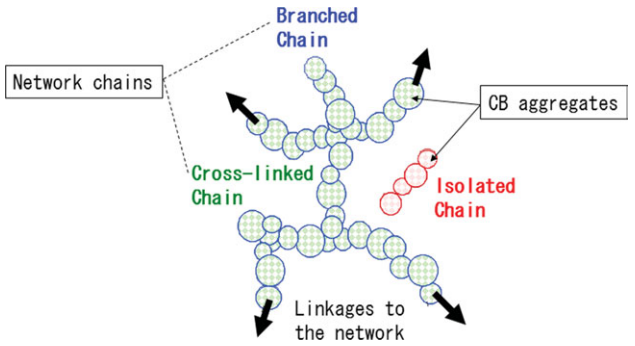

Figure 11. CB_{ag} network structure. [Color figure can be viewed in the online issue, which is available at wileyonlinelibrary.com.]

the crosslinking point (N_d) and the branching point (T_m) of the network, respectively. Presumably, this 3D network structure of the CB_{ag}'s was also closely related to various properties, in addition to the electrical characteristics. We noted that the branched chains and isolated chains of the CB_{ag}'s were observed in all of the samples that we examined. The CB_{net} parameters, that is, the fraction of crosslinked chains (F_{cross}), fraction of branched chains (F_{branch}), and fraction of isolated chains ($F_{isolate}$), were defined by the following equations.[7–14,23–27]

$$F_{cross} = NN_dN_d/(NN_dN_d + NN_dT_m + NN_i) \quad (1)$$

$$F_{branch} = NN_dT_m/(NN_dN_d + NN_dT_m + NN_i) \quad (2)$$

$$F_{isolate} = NN_i/(NN_dN_d + NN_dT_m + NN_i) \quad (3)$$

where NN_dN_d is the number of crosslinked chains, NN_dT_m is the number of branched chains, NN_i is the number of isolated chains, and $NN_dN_d + NN_dT_m + NN_i$ is the total number of network chains. The three fractions shown in eqs. (1), (2), and (3) were the parameters used to characterize the CB_{net} structure.

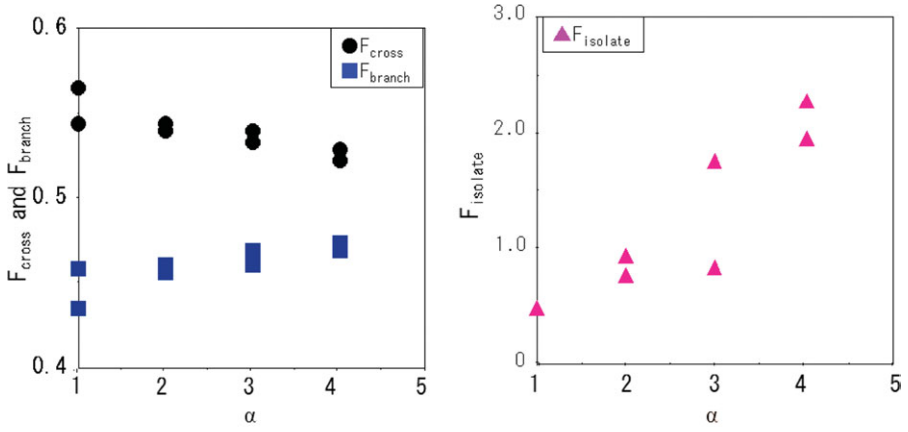

(a) Dependence of fractions of cross-linked chain (F_{cross}) and branched chain (F_{branch}) on α

(b) Dependence of fraction of isolated chain ($F_{isolate}$) on α

Figure 12. Dependence of the CB_{net} parameters on α. [Color figure can be viewed in the online issue, which is available at wileyonlinelibrary.com.]

Figure 12 shows the dependence of F_{cross}, F_{branch}, and $F_{isolate}$ on α. We observed that F_{cross} increased almost linearly and F_{branch} decreased almost linearly with increasing α. These results suggest that the crosslinked chains of the CB_{net} were severed by elongation and the number of branched chains increased. Moreover, although $F_{isolate}$ showed an overall tendency to increase with increasing α, the increase was more pronounced in the region of $3 < \alpha \leqq 4$ than in the region of $1 \leqq \alpha < 3$. These results imply that when elongation destroyed the CB_{net}, isolated chains were also generated in addition to branched chains and that the isolated chains were markedly generated in the region of $\alpha < 3$. In addition, the change in $F_{isolate}$ around $\alpha = 3$ corresponded closely to the aforementioned changes in ρ_v and ΔE and to the changes in d_p, d_g, D_{CB}, and V_{CB} of the CB_{ag}'s.

CONCLUSIONS

We observed that ρ_v of the CB40/SBR samples cured in two steps with αs of 1–3, respectively, declined slightly, whereas ρ_v of the CB40/SBR sample with an α of 4 increased markedly. These results imply that the electrical network of the CB_{ag}'s in the rubber was destroyed at $\alpha = 4$, that is, at an α larger than 3.

On the other hand, the 3D TEM images of the CB40/SBR samples cured in two steps with αs of 1–4, respectively, revealed that the gaps between the CB_{ag}'s tended to increase with increasing α. The sample with an α of 4 in particular showed that the CB_{ag}'s were broken apart. These results supported the pronounced increase in ρ_v for an α of 4. Visualized images of the CB_{net} in the CB40/SBR samples cured in two steps with αs of 1–4 showed that nearly all of the CB_{ag}'s were linked together at the closest d_p of approximately 3 nm in the unelongated state ($\alpha = 1$). In contrast, in the elongated samples, we assumed that the CB_{net} was broken as a result of elongation. For the CB40/SBR sample with an α of 4 in particular, we observed that the CB_{net} was broken up into small fragments. We found that the FD calculated with the box counting method tended to decrease with increasing α. This result presumably indicated that the CB_{net} was flattened as a result of elongation. It was also found that F_{cross} of the CB_{net} increased nearly linearly with increasing α, whereas F_{branch} decreased almost linearly. These results imply that the crosslinked chains of the CB_{net} were broken by elongation and that the number of branched chains increased. In contrast, $F_{isolate}$ tended to increase overall with increasing α; the increase in $F_{isolate}$ was more pronounced in the region of $3 < \alpha \leqq 4$ than in the region of $1 \leqq \alpha < 3$. These results suggest that when the CB_{net} was destroyed by elongation, isolated chains were also generated in addition to the branched chains. The change seen in $F_{isolate}$ around $\alpha = 3$ corresponded closely to the aforementioned changes in ρ_v and ΔE and also to the changes in d_p, d_g, the coarsened CB_{ag}'s, D_{CB}, and V_{CB}.

The foregoing results imply that the CB_{ag}'s coarsened when the sample cross-sectional area at $\alpha < 3$ decreased, and the destruction of the CB_{net} also proceeded gradually at the same time. In contrast, the coarsened CB_{ag}'s were finely divided at $\alpha > 3$, and the elongation presumably flattened and broke the CB_{net}. These results supported the marked decline observed in ρ_v at $\alpha = 4$.

ACKNOWLEDGMENTS

The authors thank H. Sawabe, A. Isoda, and Y. Takahashi of NISSAN ARC, Ltd., for their valuable cooperation with this research.

REFERENCES

1. Wei, L.; Tang, T.; Huang, B. *J. Polym. Sci. Part A: Polym. Chem.* **2004,** *42*, 941.
2. Zhang, Q.; Archer, L. *Macromolecules* **2004**, *37*, 1928.
3. Zhang, Q.; Archer, L. *Langmuir* **2002,** *18*, 10435.
4. Steinstein, S. S.; Zhu, A. *Macromolecules* **2002,** *35*, 7262.
5. Zhu, Z.; Thompson, T.; Wang, S. Q.; von Meerwall, E. D.; Halasa, A. *Macromolecules* **2005,** *38*, 8816.
6. Ozisik, R.; Zheng, J.; Dionne, P. J.; Picu, C. R.; von Meerwall, E. D. *J. Chem. Phys.* **2005,** *123*, 134901.
7. Kohjiya, S.; Kato, A.; Shimanuki, J.; Hasegawa, T.; Ikeda, Y. *J. Mater. Sci.* **2005,** *40*, 2553.
8. Kohjiya, S.; Kato, A.; Suda, T.; Shimanuki, J.; Ikeda, Y. *Polymer* **2006,** *47*, 3298.
9. Kato, A.; Shimanuki, J.; Kohjiya, S.; Ikeda, Y. *Rubber Chem. Technol.* **2006,** *79*, 653.
10. Ikeda, Y.; Kato, A.; Shimanuki, J.; Kohjiya, S.; Tosaka, M.; Poompradub, S.; Toki, S.; Hsiao, B. S. *Rubber Chem. Technol.* **2007,** *80*, 251.
11. Kohjiya, S.; Ikeda, Y.; Kato, A. In Current Topics in Elastomers Research; Bhowmick, A. K., Ed.; CRC: Boca Raton, FL, **2008; Chapter 19**, p 543.
12. Kohjiya, S.; Kato, A.; Ikeda, Y. *Prog. Polym. Sci.* **2008,** *33*, 979.
13. Omnés, B.; Thuillier, S.; Pilvin, P.; Grohens, Y.; Guillet, S. *Compos. A* **2008,** *39*, 1141.
14. Kato, A.; Suda, T.; Ikeda, Y.; Kohjiya, S. *J. Appl. Polym. Sci.* **2011,** *122*, 1300.
15. Satoh, Y.; Fujii, S.; Kawahara, S.; Isono, Y.; Kagami, S. *e-J. Soft Mater.* **2007,** *3*, 29.
16. Satoh, Y.; Suda, K.; Fujii, S.; Kawahara, S.; Isono, Y.; Kagami, S. *e-J. Soft Mater.* **2007,** *3*, 14.
17. The Carbon Black Association, Japan. Handbook of Carbon Black (in Japanese); The Carbon Black Association, Japan: Tokyo, **1995**; p 66.
18. Nihon Gosei Gomu Co., Ltd. JSR Handbook (in Japanese); JSR: Tokyo, **1985**; p 70.
19. Kremer, J. R.; Mastronarde, D. N.; McIntosh, J. R. *J. Struct. Biol.* **1996**, *116*, 71.
20. Detlev, S.; Malte, W.; Hans-Christian, H. The Visualization Handbook; Ed. Hansen, C. D.; Johnson, C. R., Ed.; Elsevier: Amsterdam, New York and Rio de Janeiro, FL, **2005**, Chapter 38, p 749.
21. Jinnai, K.; Nishi, T. *Microsc.* **2004**, *39*, 31 (in Japanese).
22. Ikeda, Y.; Kato, A.; Shimanuki, J.; Kohjiya, S. *Macromol. Rapid Commun.* **2004,** *25*, 1186.
23. Ikeda, Y. *Sen'I Gakkaishi* **2005,** *61*, 34.

24. Kato, A.; Ikeda, Y.; Kohjiya, S. *Nippon Gomu Kyokaishi* **2005,** *78*, 180.
25. Kohjiya, S.; Kato, A.; Shimanuki, J.; Hasegawa, T.; Ikeda, Y. *Polymer* **2005,** *46*, 4440.
26. Kohjiya, S.; Kato, A. *Kobunshi Ronbunshu* **2005,** *62*, 467.
27. Kato, A.; Kohjiya, S.; Ikeda, Y. *Koubunshi* **2006,** *55*, 616.
28. Kato, A.; Kohjiya, S.; Ikeda, Y. *Rubber Chem. Technol.* **2007,** *80*, 690.
29. Tsuji, M.; Fujita, M.; Kohjiya, S. *Nihon Reorogi Gakkaishi* **1997,** *25*, 193.
30. Hirata, M. *J. Appl. Polym. Sci.* **2000,** *78*, 1555.
31. Usui, M. H.; Ishizuki, M.; Shige, I.; Suzuki, H. *Korea–Aust. Rheol. J.* **2003,** *15*, 19.
32. Jäger, K.-M.; McQueen, D. H. *Polymer* **2001,** *42*, 9575.
33. Yuan, S.; Xu, H.; Gu, H. *J. Appl. Polym. Sci.* **2008, 110, 1955.**